

Misfit Stresses Due to a Cylindrical Dilatational Inclusion of Annular-Sector Cross-Section in an Infinite Elastic Medium

Zh.V. Gudkina^{1,2}, S.A. Krasnitckii^{1,3,4} and M.Yu. Gutkin^{1,3,4}

¹ITMO University, Kronverksky 49 A, St. Petersburg, 197101, Russia

²Ioffe Physical-Technical Institute, Russian Academy of Sciences, Polytekhnicheskaya 26, St. Petersburg, 194021, Russia

³Institute for Problems in Mechanical Engineering, Russian Academy of Sciences, Bolshoi 61, Vasil. Ostrov, St. Petersburg, 199178, Russia

⁴Peter the Great St. Petersburg Polytechnic University, Polytekhnicheskaya 29, St. Petersburg, 195251, Russia

Received: December 10, 2021

Abstract. An elastic model for a cylindrical dilatational inclusion of annular-sector cross-section in an infinite elastic medium is considered. The stress fields are found in a closed analytical form and are illustrated by stress maps. Specific features in the stress distribution are revealed and discussed in detail. It is shown that the stress magnitude can be so high that various mechanisms of stress relaxation can be activated.

1. INTRODUCTION

The study of inclusions is of significance to the development of advanced materials for aerospace, marine, automotive and many other applications [1]. This is because the presence of inclusions in materials affects their elastic fields at the local and the global scale and thus greatly influences their mechanical and physical properties. Since the pioneering work on an ellipsoidal inclusion in an infinite space [2], extensive research has been devoted to this area.

Analysis of elastic strains induced by misfitting inclusions in an infinite or semi-infinite elastic medium is a fundamental physical and engineering problem [3]. It has been originally done within the context of thermoelasticity and mechanics of solids [4–7] and then in seismology and geophysics [8–11]. Reviews of earlier research on this subject can be found in Refs. [12,13].

Nowadays, in parallel with further efforts on searching new solutions for inclusions and inhomogeneities of various shapes in different media within the

mechanics [1,3,14], much attention is paid to their applications in materials science [15,16] and solid-state physics [17] with special focus on structural and functional nanocomposites [18] and nanoheterostructures for electronics, optoelectronics, photonics, etc. [19]. In particular, of great interest are the inclusions of the shape different from the well-known classical cases of spheroidal, ellipsoidal, cuboidal, cylindrical, polyhedral and prismatic shapes. For example, polyspherical [20], toroidal [18,21], truncated spherical [22] and truncated cylindrical [23] inclusions have been investigated in recent years. In due course of this trends, we suggest in the present paper a solution for a cylindrical dilatational inclusion of annular-sector cross-section in an elastic infinite medium. The solution has been found by simple integration of the solution for an infinite dilatational line (i.e., a straight line subjected to 3D dilatational eigenstrain [24]) over the cross-section area of the inclusion. We show and discuss the stress fields of the inclusion as well as some possible mechanisms of their relaxation through generation of various defect configurations.

Corresponding author: Zh.V. Gudkina, e-mail: gudkinazhanna@mail.ru

2. MODEL

Consider an elastic model for a cylindrical dilatational inclusion of annular-sector cross-section (Fig. 1) in an infinite medium (matrix). Let the inclusion occupy a domain ($a < r < b$, $\theta_1 < \varphi < \theta_2$, $-\infty < z < \infty$) and its elastic constants be isotropic and equal to those of the surrounding matrix. The inclusion domain is a subject of a 3D homogeneous dilatational eigenstrain ε^* .

To obtain the stress fields due to the inclusion, we can use the corresponding stress fields of a dilatational line (Fig. 1a) in polar coordinates (r , φ), which have the following form [24]:

$$\sigma_{rr}^{(dl)} = -\alpha s \frac{r^2 - 2r r_0 \cos(\theta - \varphi) + r_0^2 \cos 2(\theta - \varphi)}{[r^2 + r_0^2 - 2r r_0 \cos(\theta - \varphi)]^2}, \quad (1a)$$

$$\sigma_{\varphi\varphi}^{(dl)} = \alpha s \frac{r^2 - 2r r_0 \cos(\theta - \varphi) + r_0^2 \cos 2(\theta - \varphi)}{[r^2 + r_0^2 - 2r r_0 \cos(\theta - \varphi)]^2}, \quad (1b)$$

$$\sigma_{r\varphi}^{(dl)} = -\alpha s \frac{2r_0[-r + r_0 \cos(\theta - \varphi)] \sin(\theta - \varphi)}{[r^2 + r_0^2 - 2r r_0 \cos(\theta - \varphi)]^2}, \quad (1c)$$

where $\alpha = G\varepsilon(1+\nu)/(1-\nu)$, G and ν are the shear modulus and the Poisson ratio, respectively, r_0 and θ are the polar coordinates of the dilatational line, s is an infinitesimal parameter corresponding to the cross-sectional area of the dilatational line.

With Eqs. (1), the stress fields created by the inclusion are determined by integrating the stress fields of the dilatational lines continuously distributed with the constant density $\rho = 1/s$ over the inclusion area S :

$$\sigma_{ij} = \iint_S \sigma_{ij}^{(dl)} \rho dS. \quad (2)$$

Substitution of Eqs. (1) to Eq. (2) gives the integral representation of the inclusion stress fields as follows:

$$\begin{aligned} \sigma_{rr} = & -\alpha \\ & \times \int_{\theta_1}^{\theta_2} \int_a^b \frac{r^2 - 2r r_0 \cos(\theta - \varphi) + r_0^2 \cos 2(\theta - \varphi)}{[r^2 + r_0^2 - 2r r_0 \cos(\theta - \varphi)]^2} r_0 dr_0 d\theta, \end{aligned} \quad (3a)$$

$$\begin{aligned} \sigma_{\varphi\varphi} = & \alpha \\ & \times \int_{\theta_1}^{\theta_2} \int_a^b \frac{r^2 - 2r r_0 \cos(\theta - \varphi) + r_0^2 \cos 2(\theta - \varphi)}{[r^2 + r_0^2 - 2r r_0 \cos(\theta - \varphi)]^2} r_0 dr_0 d\theta, \end{aligned} \quad (3b)$$

$$\begin{aligned} \sigma_{r\varphi} = & -2\alpha \int_{\theta_1}^{\theta_2} \int_a^b \frac{r_0[-r + r_0 \cos(\theta - \varphi)] \sin(\theta - \varphi)}{[r^2 + r_0^2 - 2r r_0 \cos(\theta - \varphi)]^2} r_0 dr_0 d\theta. \end{aligned} \quad (3c)$$

After analytical integration, these stress components take the following closed form:

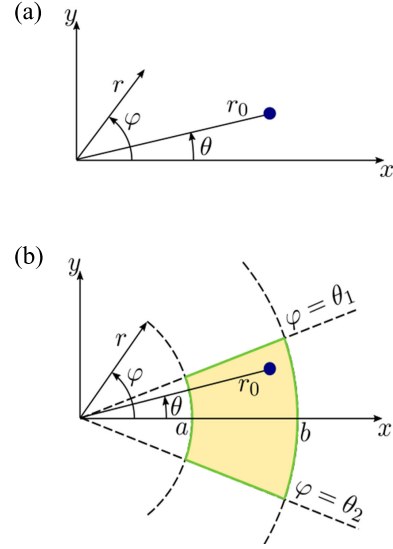


Fig. 1. Elastic models in polar (r , φ) and Cartesian (x , y) coordinates: (a) a dilatational line in an infinite medium, (b) a dilatational line and a cylindrical dilatational inclusion of annular-sector cross-section in an infinite medium.

$$\begin{aligned} \sigma_{rr} = & \frac{\alpha}{4r^2} \left\{ r_0^2 (\theta - \varphi) + 4r_0^2 \arctan \left(\frac{r - r_0}{r + r_0} \cot \frac{\theta - \varphi}{2} \right) \right. \\ & + 2r_0^2 \arctan \left(\frac{r + r_0}{r - r_0} \tan \frac{\theta - \varphi}{2} \right) - 2r r_0 \sin(\theta - \varphi) \\ & + 2r^2 \arctan \frac{r \cos(\theta - \varphi) - r_0}{r \sin(\theta - \varphi)} \cos 2(\theta - \varphi) \\ & \left. - r^2 [1 + \ln(r^2 - 2r r_0 \cos(\theta - \varphi) + r_0^2)] \right. \\ & \left. \times \sin 2(\theta - \varphi) \right\} \Bigg|_{r_0=a}^{r_0=b} \Bigg|_{\theta=\theta_1}^{\theta=\theta_2} - \pi H(r-1.5) H(\varphi), \end{aligned} \quad (4a)$$

$$\begin{aligned} \sigma_{\varphi\varphi} = & -\frac{\alpha}{4r^2} \left\{ r_0^2 (\theta - \varphi) + 4r_0^2 \arctan \left(\frac{r - r_0}{r + r_0} \cot \frac{\theta - \varphi}{2} \right) \right. \\ & + 2r_0^2 \arctan \left(\frac{r + r_0}{r - r_0} \tan \frac{\theta - \varphi}{2} \right) - 2r r_0 \sin(\theta - \varphi) \\ & + 2r^2 \arctan \frac{r \cos(\theta - \varphi) - r_0}{r \sin(\theta - \varphi)} \cos 2(\theta - \varphi) \\ & \left. - r^2 [1 + \ln(r^2 - 2r r_0 \cos(\theta - \varphi) + r_0^2)] \right. \\ & \left. \times \sin 2(\theta - \varphi) \right\} \Bigg|_{r_0=a}^{r_0=b} \Bigg|_{\theta=\theta_1}^{\theta=\theta_2} - \pi H(r-1.5) H(\varphi), \end{aligned} \quad (4b)$$

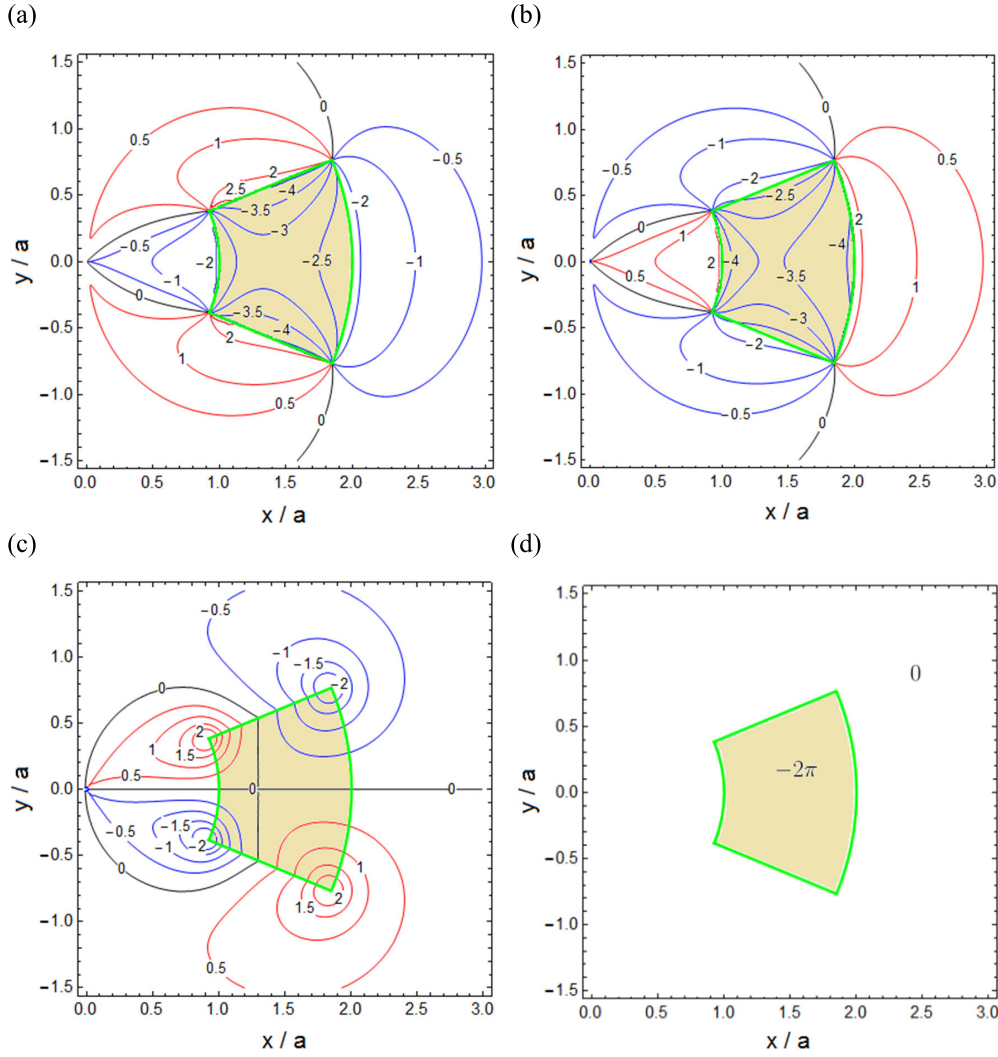


Fig. 2. Stress maps of a cylindrical dilatational inclusion of annular-sector cross-section ($a < r < b(=2a)$, $-\pi/8 < \varphi < \pi/8$) in an infinite homogeneous elastic medium: (a) σ_{rr} , (b) $\sigma_{\varphi\varphi}$, (c) $\sigma_{r\varphi}$, and (d) σ_{zz} . The stress values are given in units of α . The green line shows a cross-section of the inclusion.

$$\begin{aligned}
 \sigma_{r\varphi} = & \frac{\alpha}{4r^2} \left\{ r^2 \cos 2(\theta - \varphi) + 2r r_0 \cos(\theta - \varphi) \right. \\
 & + 2r^2 \arctan \frac{r \cos(\theta - \varphi) - r_0}{r \sin(\theta - \varphi)} \sin 2(\theta - \varphi) \\
 & + [r_0^2 + r^2 \cos 2(\theta - \varphi)] \\
 & \left. \times \ln [r^2 - 2r r_0 \cos(\theta - \varphi) + r_0^2] \right\} \Big|_{r_0=a}^{r_0=b} \Big|_{\theta=\theta_1}^{\theta=\theta_2}. \quad (4c)
 \end{aligned}$$

where $H(t)$ is the Heaviside function.

3. RESULTS

Fig. 2 shows the maps of the nonvanishing stress components caused by the inclusion with the cross-section domain ($a < r < b(=2a)$, $-\pi/8 < \varphi < \pi/8$) highlighted by the green contour.

As is seen from Fig. 2, the maps of normal stress components σ_{rr} , $\sigma_{\varphi\varphi}$, and σ_{zz} are symmetric with respect to the x -axis, while that of the shear stress $\sigma_{r\varphi}$ is antisymmetric. Fig. 2a shows that the radial stress σ_{rr} is continuous at the interfaces $r = a$ and $r = 2a$. For a positive value of ε^* , the highest tensile radial stress ($\sigma_{rr,\max} \approx 2.5\alpha$) is achieved in the matrix near the left vertices ($x \approx 0.9a$, $y \approx \pm 0.4a$) of the inclusion, while the highest compressive radial stress ($\sigma_{rr,\min} \approx -4\alpha$) is achieved in the inclusion near its right vertices ($x \approx 1.85a$, $y \approx \pm 0.8a$). For an exemplary set of material parameters, $\varepsilon^* = 0.01$ and $\nu = 0.3$, the value of α is roughly $\alpha \approx G/54$ that gives $\sigma_{rr,\max} \approx G/22$ and $\sigma_{rr,\min} \approx -G/14$. These stress levels are obviously very high. It is of interest that they occur at the flat segments of the interface, which could hardly be predicted.

Figure 2b shows that the hoop stress $\sigma_{\varphi\varphi}$ is continuous at the interfaces $\varphi = \pm\pi/8$. When eigenstrain ε^* is positive, the highest tensile hoop stress ($\sigma_{\varphi\varphi,\max} \approx 2\alpha$) is reached in the matrix near the curved segments of the interface, while the highest compressive hoop stress ($\sigma_{\varphi\varphi,\min} \approx -4\alpha$) is reached in the inclusion near the same curved segments of the interface. At $\alpha \approx G/54$, one can estimate $\sigma_{\varphi\varphi,\max} \approx G/27$ and $\sigma_{\varphi\varphi,\min} \approx -G/14$. These are very high stress levels. In contrast to the case of radial stress, these extremal stress levels are characteristic for the curved segments of the interface.

It is seen from Fig. 2c that the shear stress $\sigma_{r\varphi}$ is continuous across all segments of the interface and has singularities at the inclusion vertices as is the case with similar inclusions of rectangular cross section within the classical linear elasticity [25]. One can deal with this classical singularity using, for example, strain-gradient elasticity theory [26]. Nevertheless, the inclusion vertices remain the points of shear stress concentration even in the latter case. It is of interest here, that in the case of partially curvilinear interface, the stress gradient is higher in vicinity of the left vertices than in vicinity of the right ones. Therefore, the right vertices bounding the longer curved segment of the interface, can be considered as stronger stress concentrators than the left vertices bounding its shorter curved segment.

Fig. 2d demonstrates that the axial stress σ_{zz} is constant and equal to $-2\pi\alpha$ (for $\alpha \approx G/54$ this gives the extremely high compressive stress $\sigma_{zz} \approx G/9$) inside the inclusion and equal to zero in the matrix. For the hydrostatic stress component $\sigma = \sigma_{ii}/3 = 2\sigma_{zz}/3$, this provides a similar well-known result that σ is constant inside the inclusion and equal to zero outside, which is true for any shape of the inclusion placed in an infinite matrix [2].

Based on the aforementioned features in the stress field distribution inside and around the inclusion, one can expect that the most probable channels of the stress relaxation can be generation of either (i) prismatic dislocation loops of arbitrary shape inside the inclusion in its cross section or (ii) dipoles of edge dislocations emitted by the right vertices of the inclusion and gliding along the straight segments of the interface in such a way that one of these dislocation would stop near the zero-value contours of the shear stress $\sigma_{r\varphi}$ at the interface (see Fig. 2c), while the other one would stop somewhere in the matrix in vicinity of the point of its emission. A quantitative description of these mechanisms requires a special theoretical examination similar to those given recently in Refs. [27, 28].

4. CONCLUSIONS

The stress fields caused by a cylindrical dilatational inclusion of annular-sector cross-section in an infinite elastic medium are found in a closed analytical form by simple integration of the well-known stress fields of a dilatational line over the inclusion cross-section area. The solution found is illustrated by maps of all non-vanishing stress components that allow to reveal new interesting features in the stress distribution inside and outside the inclusion. It is shown that, in the exemplary case of a positive eigenstrain of the inclusion, (i) the radial stress achieves its extremal values at the flat segments of the interface, the highest tensile stress in the matrix near the vertices restricting the shorter curved segment of the interface, while the highest compressive stress in the inclusion near its vertices restricting the longer curved segment of the interface; (ii) the hoop stress reaches its extremal values in the central regions of the curved segments of the interface, the highest tensile stress in the matrix, while the highest compressive stress in the inclusion; (iii) the shear stress is singular at the inclusion vertices and the shear stress gradient is higher in vicinity of the vertices restricting the shorter curved segment of the interface, than in vicinity of the vertices restricting its longer curved segment; (iv) both the axial and hydrostatic stresses are constant inside the inclusion and equal to zero in the matrix; (v) for reasonable values of the model parameters, $\varepsilon^* = 0.01$ and $\nu = 0.3$, the stress magnitude can reach rather high levels from $G/27$ to $G/9$ depending on the stress component. Based on the results listed above, one can conclude that suitable theoretical models for stress relaxation in/around the inclusion are highly desired.

REFERENCES

- [1] K. Zhou, H.J. Hoh, X. Wang, L.M. Keer, J.H. Pang, B. Song and Q.J. Wang, *A review of recent works on inclusions*, Mech. Mater., 2013, vol. 60, pp. 144–158.
<https://doi.org/10.1016/j.mechmat.2013.01.005>
- [2] J.D. Eshelby, *The determination of the elastic field of an ellipsoidal inclusion, and related problems*, Proc. R. Soc. Lond. A, 1957, vol. 241, no. 1226, pp. 376–396.
<https://doi.org/10.1098/rspa.1957.0133>
- [3] B.N. Kuvshinov, *Elastic and piezoelectric fields due to polyhedral inclusions*, Int. J. Solids Struct., 2008, vol. 45, no. 5, pp. 1352–1384.
<https://doi.org/10.1016/j.ijsolstr.2007.09.024>

- [4] R.D. Mindlin, *Force at a point in the interior of a semi-infinite solid*, *Physics*, 1936, vol. 7, no. 5, pp. 195–202.
<https://doi.org/10.1063/1.1745385>
- [5] J.N. Goodier, *On the integration of the thermoelastic equations*, *Phil. Mag.*, 1937, vol. 23, no. 157, pp. 1017–1032.
<https://doi.org/10.1080/14786443708561872>
- [6] R.D. Mindlin and D.H. Cheng, *Thermoelastic stress in the semi-infinite solid*, *J. Appl. Phys.*, 1950, vol. 21, no. 9, pp. 931–933.
<https://doi.org/10.1063/1.1699786>
- [7] B. Sen, *Note on stresses produced by nuclei of thermo-elastic strain in a semi-infinite elastic solid*, *Quatr. Appl. Math.*, 1951, vol. 8, no. 4, pp. 365–369.
<https://doi.org/10.1090/QAM/37717>
- [8] J.A. Geertsma, *A remark on the analogy between thermoelasticity and the elasticity of saturated elastic porous media*, *J. Mech. Phys. Solids*, 1957, vol. 6, no. 1, pp. 13–16.
[https://doi.org/10.1016/0022-5096\(57\)90042-X](https://doi.org/10.1016/0022-5096(57)90042-X)
- [9] J.A. Steketee, *On Volterra's dislocations in a semi-infinite elastic medium*, *Can. J. Phys.*, 1958, vol. 36, no. 2, pp. 192–205.
<https://doi.org/10.1139/p58-024>
- [10] L. Rongved and J.T. Frazier, *Displacement discontinuity in the elastic half-space*, *J. Appl. Mech.*, 1958, vol. 25, no. 1, pp. 125–128.
<https://doi.org/10.1115/1.4011700>
- [11] J. Geertsma, *Land subsidence above compacting oil and gas reservoir*, *J. Pet. Technol.*, 1973, vol. 25, no. 6, pp. 734–744.
<https://doi.org/10.2118/3730-PA>
- [12] W. Nowacki, *Thermoelasticity*, Pergamon, Oxford, 1986.
- [13] T. Mura, *Micromechanics of Defects in Solids*, Martinus Nijhoff Publishers, Dordrecht, 1987.
- [14] M. Kachanov and I. Sevostianov, *Micromechanics of Materials, with Applications*, Springer, 2018.
<https://doi.org/10.1007/978-3-319-76204-3>
- [15] M. Doi, *Elasticity effects on the microstructure of alloys containing coherent precipitates*, *Prog. Mater. Sci.*, 1996, vol. 40, no. 2, pp. 79–180.
[https://doi.org/10.1016/0079-6425\(96\)00001-1](https://doi.org/10.1016/0079-6425(96)00001-1)
- [16] X. Zhao, R. Duddu, S.P.A. Bordas and J. Qu, *Effects of elastic strain energy and interfacial stress on the equilibrium morphology of misfit particles in heterogeneous solids*, *J. Mech. Phys. Solids*, 2013, vol. 61, no. 6, pp. 1433–1445.
<https://doi.org/10.1016/j.jmps.2013.01.012>
- [17] A.P. Chernakov, A.L. Kolesnikova, M.Yu. Gutkin and A.E. Romanov, *Periodic array of misfit dislocation loops and stress relaxation in core-shell nanowires*, *Int. J. Eng. Sci.*, 2020, vol. 156, art. no. 103367.
<https://doi.org/10.1016/j.ijengsci.2020.103367>
- [18] S. Krasnitskii, A. Trofimov, E. Radi and I. Sevostianov, *Effect of a rigid toroidal inhomogeneity on the elastic properties of a composite*, *Math. Mech. Solids*, 2019, vol. 24, no. 4, pp. 1129–1146.
<https://doi.org/10.1177/1081286518773806>
- [19] F. Glas, *Strain in nanowires and nanowire heterostructures*, *Semiconductors and Semimetals*, 2015, vol. 93, pp. 79–123.
<https://doi.org/10.1016/bs.semsem.2015.09.004>
- [20] L. Lanzoni, E. Radi and I. Sevostianov, *Effect of spherical pores coalescence on the overall conductivity of a material*, *Mech. Mater.*, 2020, vol. 148, art. no. 103463.
<https://doi.org/10.1016/j.mechmat.2020.103463>
- [21] E. Radi and I. Sevostianov, *Toroidal insulating inhomogeneity in an infinite space and related problems*, *Proc. Math. Phys. Eng. Sci.*, 2016, vol. 472, no. 2187, art. no. 20150781.
<https://doi.org/10.1098/rspa.2015.0781>
- [22] A.L. Kolesnikova, M.Yu. Gutkin and A.E. Romanov, *Analytical elastic models of finite cylindrical and truncated spherical inclusions*, *Int. J. Solids Struct.*, 2018, vol. 143, pp. 59–72.
<https://doi.org/10.1016/j.ijsolstr.2018.02.032>
- [23] F. Glas, *Elastic relaxation of a truncated circular cylinder with uniform dilatational eigenstrain in a half space*, *Phys. Status Solidi B*, 2003, vol. 237, no. 2, pp. 599–610.
<https://doi.org/10.1002/pssb.200301801>
- [24] A.L. Kolesnikova, R.M. Soroka and A.E. Romanov, *Defects in the elastic continuum: classification, fields and physical analogies*, *Mater. Phys. Mech.*, 2013, vol. 17, no. 1, pp. 71–91.
<https://mpm.spbstu.ru/en/article/2013.28.11/>
- [25] K.L. Malyshev, M.Yu. Gutkin, A.E. Romanov, A.A. Sitnikova and L.M. Sorokin, *Stress fields and diffraction contrast of rod-like defects in silicon*, *Sov. Phys.-Solid State*, 1988, vol. 30, no. 7, pp. 1176–1179.
- [26] M.Yu. Gutkin, *Elastic behavior of defects in nanomaterials. I. Models for infinite and semi-infinite media*, *Rev. Adv. Mater. Sci.*, 2006, vol. 13, no. 2, pp. 125–161.
https://ipme.ru/e-journals/RAMS/no_21306/gutkin.pdf

- [27] K.N. Mikaelyan, M.Yu. Gutkin, E.N. Borodin and A.E. Romanov, *Dislocation emission from the edge of a misfitting nanowire embedded in a free-standing nanolayer*, Int. J. Solids Struct., 2019, vol. 161, pp. 127–135.
<https://doi.org/10.1016/j.ijsolstr.2018.11.014>
- [28] A.M. Smirnov, S.A. Krasnitskii and M.Yu. Gutkin, *Generation of misfit dislocations in a core-shell nanowire near the edge of prismatic core*, Acta Mater., 2020, vol. 186, pp. 494–510.
<https://doi.org/10.1016/j.actamat.2020.01.018>